Supplementary Material of *Modeling multilayer coating systems in solar receivers*

D. Chen et al.

February 2020

1 Finite Element Analysis and comparison with the analytical model

The sequential field-coupling is used assuming that the stress field in a structure depends on the temperature field in that structure, but the reverse is not significant. In such thermal-stress analysis, the nodal temperatures calculated from an uncoupled heat transfer analysis are applied as 'body force' loads in the subsequent stress/deformation analysis. The geometry is meshed with two dimensional eight-node biquadratic elements to avoid problems related to material incompressibility. The element types are Plane 77 in thermal analysis and Plane 183 in stress analysis. A structured grid is employed with a mesh size of 0.1 mm in the length (x) direction and of 0.01 mm in the thickness (z) direction. The symmetric boundary condition is applied at the left edge of the model to remove the horizontal displacement, as illustrated in Figure S4. The node at the bottom of the symmetric axis is fixed to constraint the displacement along the z direction.

The slider type multi-point constrain (MPC) is applied on the right edge using the MPC184 slider element in ANSYS (KEYOPT(1)=3). The utilization of MPC allows to connect different nodes and their degrees of freedom together. In this work, the system is considered as an infinite plate. It is desirable to constrain the nodes on the free edge (right edge) to remain in a straight line, but allow the deformation and movement of nodes along this line as well as the change in length of the line. As shown in Figure S4, a portion of the system is modeled. In theory, any cross-section should remain straight and normal to the mid-surface of the system. Without MPC or other boundary conditions, nodes on the right edge are free to deflect. It is not accurate to simulate the part of the system not included in the analysis.

Figure S2 shows the normal stress contour (σ_x) before thermal cycling (after deposition, at T_{amb}), with and without the utilization of MPC boundary condition on the right edge, respectively. The free deflection of nodes in the region

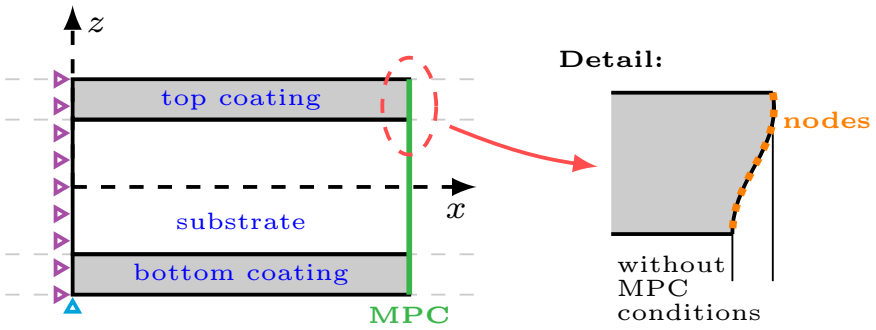

Figure S1: Schematic representation of a part of the system; boundary conditions are employed in the finite element model: violet triangles represent symmetric boundary condition and the cyan one show the constraint of vertical displacement; MPC conditions applied at the right edge to force nodes move along a straight line.

close to the right edge leads to stress relaxation along the length direction in both coating and substrate. There also exists a stress gradient along the z direction with stress concentration at the coating/substrate interface. As presented above, the slider type MPC restrains the right edge to deform as a straight line. Stress distribution is uniform in both coating and substrate, which is consistent with the thin plate theory. It is therefore confident to use the MPC boundary condition for the benchmarking.

Values of stresses of FEA prediction with MPC boundary condition (Figure S3) are in good agreement with those of the analytical model (-320 MPa in AlN layers and 38 MPa in TZM substrate). The AlN coatings exhibit compressive stresses, whereas the stress in the substrate is tensile. The stress in the coating is one order of magnitude higher than that in the substrate. This confirms the validity of the proposed model. Moreover, compared with the FEA, the analytical model can easily integrate the different high temperature phenomena such as oxidation. It is therefore confident to use the present analytical model for calculating stress evolution in multilayer coating systems during their use in solar receivers.

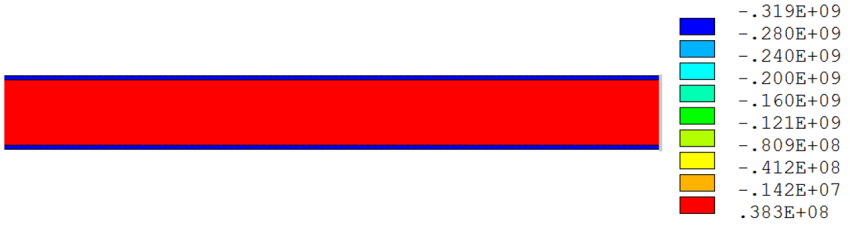

(a) Stress field after deposition, with MPC boundary condition

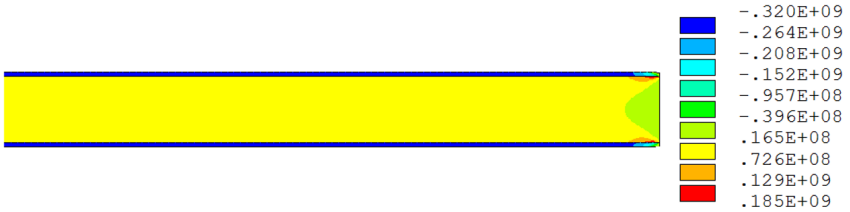

(b) Stress field after deposition, without MPC boundary condition

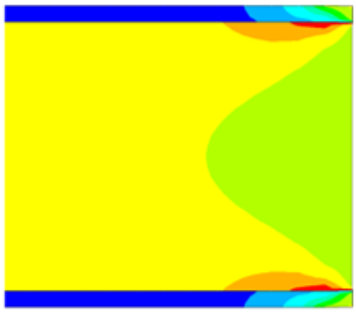

(c) High magnification of (b) at the right edge, for clarity

Figure S2: Normal stress field calculated by FEA after deposition at T_{amb}: (a) with MPC boundary condition applied at the right edge; (b) without the use of MPC boundary condition and (c) a high magnification of (b) at the right edge.

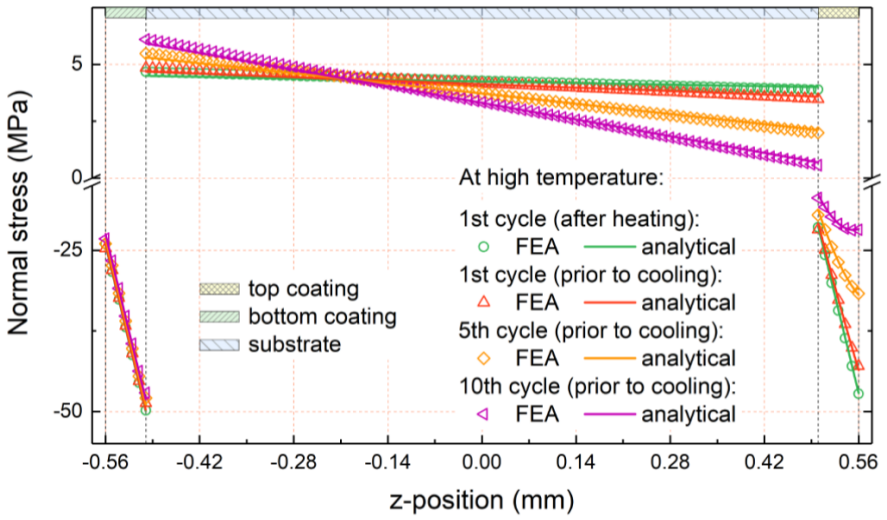

(a) Stress distribution at high temperature during the thermal cycling

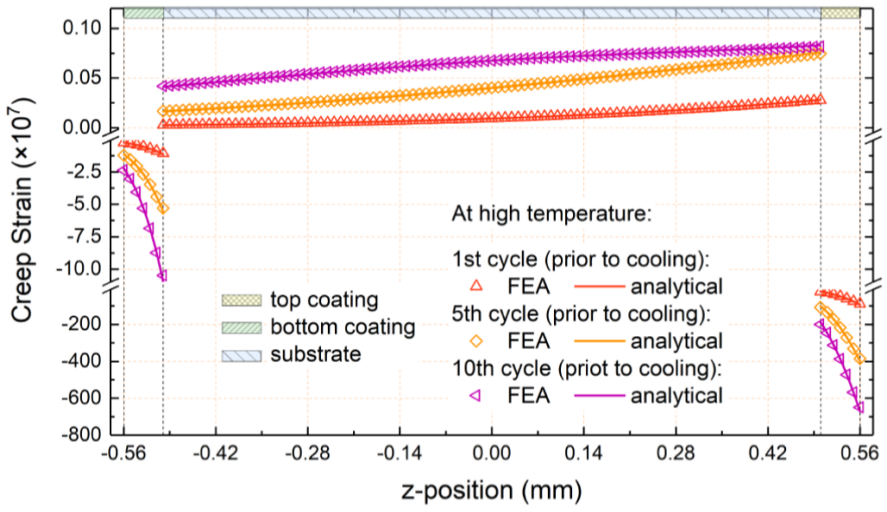

(b) Creep strain distribution at high temperature during the thermal cycling

Figure S3: Comparison between FEA and the present model: (a) normal stress and (b) creep strain distribution at the high temperature plateau

2 Stress evolution in the system with linear oxidation

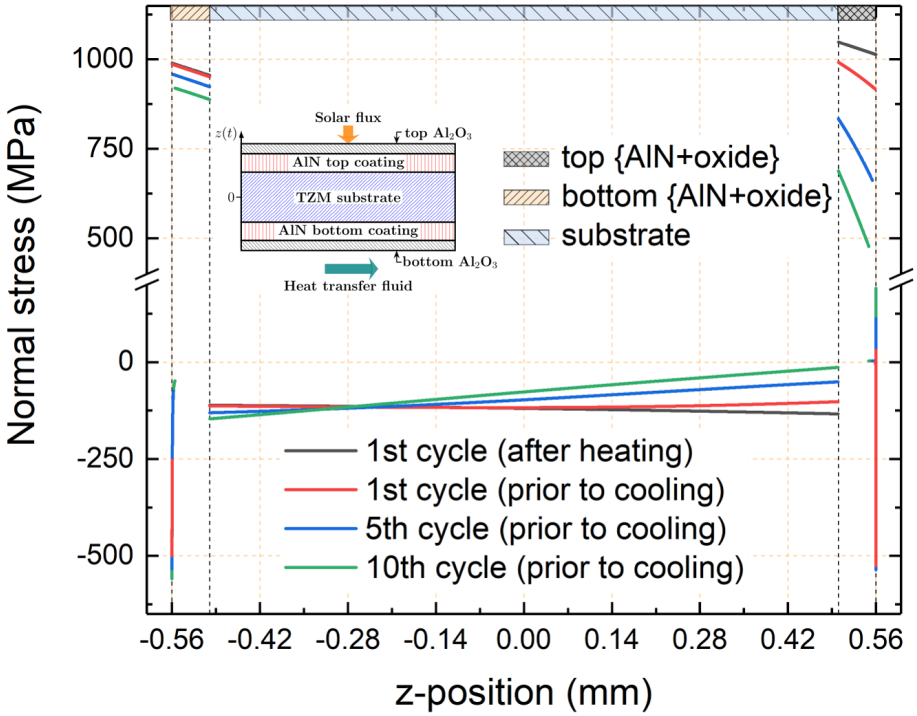

Figure S4: Normal stress distribution in the system during thermal cycling when oxide scale growth is considered

3 Linear oxidation vs parabolic oxidation

We assume here that the parabolic oxidation kinetics can be extended in the temperature range of 1000-1100 °C.

Chou and Hou [Chou(2006), Hou and Chou(2009)] have proposed a model to explicitly express the reacted fraction of oxidation, ξ as a function of oxidation duration t, such as:

$$\xi = (\frac{1}{\Theta_T} \cdot exp(-\frac{\Delta E_d}{R \cdot T}) \cdot t)^{\frac{1}{2}} \tag{1}$$

where ΔE_d is the activation energy of diffusion and Θ_T is a constant related to oxygen partial pressure. For the oxidation of AlN, the relationship between mass gain and the reacted fraction can be written as follow:

$$\xi = \frac{\Delta m}{m_0} \cdot \frac{M_{AlN}}{\frac{1}{2}M_{Al_2O_3} - M_{AlN}} \tag{2}$$

where M_{AlN} and $M_{Al_2O_3}$ are the molecular masses of AlN and Al_2O_3 respectively, and m_0 the initial mass of AlN. From oxidation experiments in the temperature range of 1327-1527 °C, values of Θ_T and ΔE_d are obtained as 5.7 s^{-1} and 2.309×10^5 $J \cdot mol^{-1}$, respectively. The lateral growth strain rate constant η_g, for the parabolic growth of oxide, is assumed to be 10×10^4 to clarify the stress evolution.

The evolution of curvature and stresses at the three representative positions are depicted in Figure S5. Stresses in the coatings and substrate are nearly unaffected by the oxidation kinetics, whereas the curvature and stress in the oxide scales have different features of evolution. Indeed, as the oxide growth is limited by diffusion, the thickness of the oxide scales is much lower than in the case of linear growth. The thermal mismatches are thus limited. The decrease of curvature at high temperature is not significant and the variation of $\Delta\frac{1}{r}|_{HT \to T_{amb}}$ is reduced. In the oxide scales, we observe an increase and a subsequent decrease of stress. This results from the competition between the accumulation of compressive creep strain and development of lateral strain in the oxide scales. At the end of thermal cycling, stresses in the oxide scales are relaxed to reach a constant ($\sim$-0.5 GPa), which means that a steady competition exists between stress build-up (constraint of the lateral expansion) and stress relaxation (upon creep deformation).

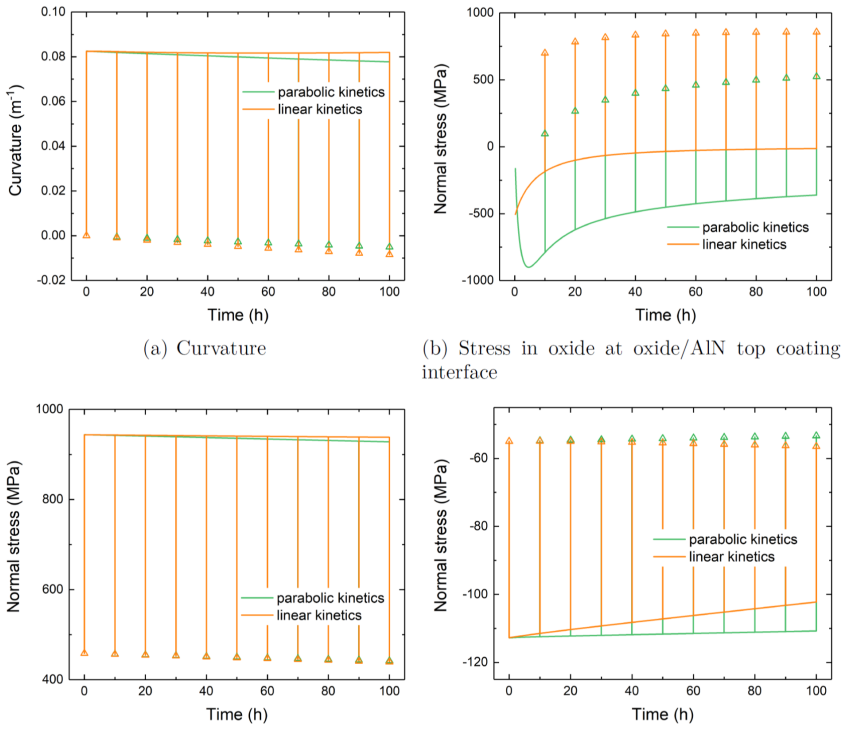

(a) Curvature

(b) Stress in oxide at oxide/AlN top coating interface

(c) Stress in coating at AlN top coating/substrate interface

(d) Stress at the center of the substrate

Figure S5: Effect of oxide scale growth kinetics on (a) evolution of the curvature of the system, and stress evolution at (b) oxide/AlN top coating interface (on oxide side), (c) AlN top coating/substrate interface (on coating side) and (d) the center of substrate; triangles represent the curvature and/or stresses at ambient temperature

4 Effect of residual stress during coating deposition

Stress in coating can be controlled by the microstructure and the deposition conditions. Here, the residual CVD growth stress, σ_g, is ranged from 430 to 1290 MPa in AlN top and bottom coatings. The heat transfer fluid and the heat flux are respectively set to 1000°C and 1 MW·m^{-2}. Figure S6 show that the evolution of curvature and stress in the oxide scale are almost not affected by the value of residual stress. The residual stress only influence the thermoelastic response of the system which remains almost constant till the end of thermal cycling.

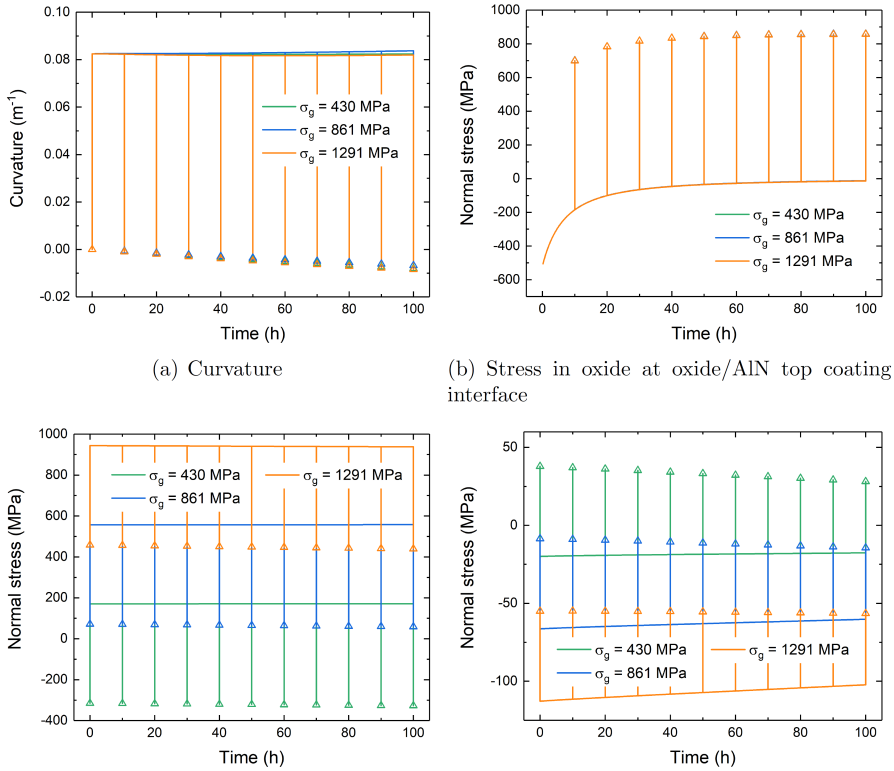

(a) Curvature

(b) Stress in oxide at oxide/AlN top coating interface

(c) Stress in coating at AlN top coating/substrate interface

(d) Stress at the center of the substrate

Figure S6: Effect of intrinsic CVD growth stress in AlN coatings on (a) evolutions of the curvature of the system, and stress evolutions at (b) oxide/AlN top coating interface (on oxide side), (c) AlN top coating/substrate interface (on coating side) and (d) the center of substrate; triangles represent the curvature and/or stresses at ambient temperature.

References

[Chou(2006)] K.-C. Chou, Journal of the American Ceramic Society 89 (2006) 1568 – 1576. URL: https://ceramics.onlinelibrary.wiley.com/doi/abs/10.1111/j.1551-2916.2006.00959.x. doi:10.1111/j.1551-2916.2006.00959.x. arXiv:https://ceramics.onlinelibrary.wiley.com/doi/pdf/10

[Hou and Chou(2009)] X. Hou, K.-C. Chou, Corrosion Science 51 (2009) 556 -- 561. URL: http://www.sciencedirect.com/science/article/pii/S0010938X0800532 doi:https://doi.org/10.1016/j.corsci.2008.12.007.